J Electroceram (2007) 18:323–327
DOI 10.1007/s10832-007-9175-6

Electrical properties of $Pb_{0.98}Eu_{0.02}(Zr_yTi_{1-y})_{0.995}O_3$ prepared by sol–gel processing

Federico González · María-Elena Villafuerte-Castrejón · Alfonso Huanosta

Published online: 26 May 2007

Abstract A $Pb_{0.98}Eu_{0.02}(Zr_yTi_{1-y})_{0.995}O_3$ compound series, with y=0.60, 0.53 and 0.45 was prepared. PZT samples were synthesized by sol–gel technique. The crystallization and quality of the compounds were analyzed by powder X-ray diffraction and electron microscopy. The shape of the $\varepsilon'(\omega)$ vs T curves can be considered typical of a ferro-paraelectric transition. The ferro-paraelectric transition temperature for each composition was 348, 328 and 307°C, for the y=0.45, 0.53 and 0.60, respectively. $\sigma'(\omega)$ is strongly influenced by short range processes. For the $\log\sigma'(\omega)$ curves as function of temperature, there is evidence of a non dispersive dc-conductivity component for the high temperature region. The associated dc-activation energies are larger than those calculated for the ac region (at lower temperatures).

Keywords PZT · Ferroelectric properties · Sol gel processing

1 Introduction

There has been great interest in the solid solution of lead zirconate titanate $PbZr_xTi_{1-x}O_3$ (PZT), due to its capacity for ferroelectric behavior [1–3]. Ferroelectric ceramics are being widely used for forefront applications in areas of research, as well as in industrial applications, such as thermal detectors, thermal imaging, high dielectric capacitors, computer memory and display, transducers and sensors [2–6].

F. González (✉) · M.-E. Villafuerte-Castrejón · A. Huanosta
Instituto de Investigaciones en Materiales,
Universidad Nacional Autonoma de Mexico,
A. P. 70-360 Mexico D.F., Mexico
e-mail: federico@iim.unam.mx

PZT, with a perovskite ABO_3 type structure, has been doped with different ions. In particular, the incorporation of rare earths improves and optimizes their properties. On the other hand, it has been found that the properties of PZT are sensitive to its compositional fluctuations, particle size, doping, calcinations and sintering temperature. Recently, sol gel processing of ceramics has attracted greater interest, due to its intrinsic advantages as compared to other conventional processing techniques. The sol–gel process allows low calcinations and sintering temperature, a high degree of molecular mixing, chemical homogeneity and good control of stoichiometry.

Although several works have been carried out on europium modified PZT, no reports have been forthcoming on the effect of substituting Eu^{3+} with various Zr/Ti ratios. The aim of this work is to report the systematic comparative study of the crystal structures, microstructures and dielectric properties, in order to provide a better understanding of phase transition in sol–gel grown doped PZT ceramics; $Pb_{0.98}Eu_{0.02}(Zr_yTi_{1-y})_{0.995}O_3$, y=0.60, 0.53 and 0.45.

2 Experimental

Polycrystalline PZT samples were synthesized by sol–gel technique. Acetate alkoxide gels were prepared from lead acetate trihydrate $Pb(CH_3COO)_2{\cdot}3H_2O$ (99.9+%), europium (III) nitrate pentahydrate $Eu(NO_3)_3{\cdot}5H_2O$ (99.9%), zirconium propoxide $Zr(C_3H_7O)_4$ (70% in 1-propanol) and titanium isopropoxide $Ti[(CH_3)_2CHO]_4$ (99.999%). Glacial acetic acid (99.8%) and deionized water were used as solvents, employing the process modifications of Yi et al. [7]. The solution was dried for 36 h at 200°C. The dried powdered gels were annealed at 900°C for 1 h, in order to precipitate the crystalline phase. After the annealing, the

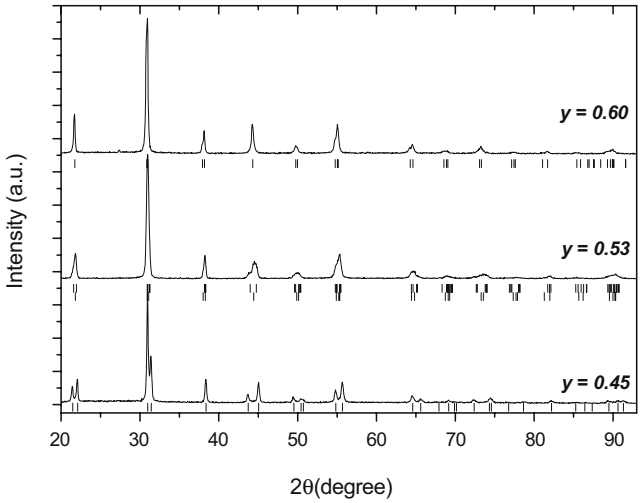

Fig. 1 XRD patterns of the $Pb_{0.98}Eu_{0.02}(Zr_yTi_{1-y})_{0.995}O_3$ samples with different compositions (all sintered at 1200°C). The *thick marks* correspond to the crystalline phases present in each sample

powders were cold pressed to form disk shaped pellets (10 mm in diameter, 1 mm in thickness), under a load of 35 MPa, using a uniaxial hydraulic press. The pellets were then sintered at 1200°C for 2 h. To prevent lead loss by vaporization during sintering, a Pb vapor pressure was established using a mixture of $PbZrO_3$ and PbO (10%), and by placing everything in a covered alumina crucible to maintain the stoichiometry of the compounds. Two pellets of each composition were annealed at the same conditions, i.e., at 1200°C for 2 h. One of the pellets was used for the electrical measurements, and the other was used for the scanning electron microscopy (SEM), density measurements, and X-ray diffraction (XRD) technique. The samples were observed in a (JEOL™) scanning electron microscopy JSM 5600-LV. Specimens were prepared by fracturing the pellets. The precipitation and quality of the compounds were checked by X-ray diffraction (XRD), using a powder diffractometer. The patterns, obtained by grinding the ceramic samples, were recorded at room temperature with CuKα radiation, in a Bruker Advanced D-8 diffractometer. Diffraction intensity was measured between 15° and 110°, with a 2θ step of 0.02° for 4 s per point.

In order to investigate dielectric properties, air drying silver conductive (from SPI) was applied to the parallel faces, so as to obtain a two-probe configuration. For impedance measurements, a Hewlett Packard 4192A impedance analyzer was used; data being collected over the frequency range of 5 to 13 MHz. Runs were taken in 6–8°C steps in proximity to the transition temperature; otherwise the steps were 20–30°C. The rms applied voltage was 1 V. In order to allow thermal equilibrium, samples were left at the preset temperature for at least 60 min between measurements. Experiments were performed from room temperature up to 600°C in air.

3 Results and discussion

The XRD patterns of the grounded sintered pellets (Fig. 1), for the three compositions, show the formation of different crystalline phases corresponding to the perovskite-type structure: rhombohedral for y=0.60; monoclinic and rhombohedral for y=0.53; and tetragonal for y=0.45. Some previous papers report the presence of the pyrochlore-type structure in PZT doped with rare earths [8, 9], and specifically with europium [10]. However, no evidence of this phase was observed in our samples. This can be attributed to the better homogeneity obtained by the selected route of synthesis and the previous heat treatment in order to obtain the crystalline phase. The Rietveld refinement confirmed the crystalline structure and allowed the cell parameters measurement for each composition (Table 1). This table also shows the experimental and theoretical densities, along with the average grain sizes.

In the PZT compound, the addition of Nd^{3+} inhibits [11] crystalline grain growth. In this work, maintaining the Eu^{3+} content constant, we investigated how the variation of the Zr/Ti ratio affects grain growth. We recorded two incidences of grain growth enlargement, induced by the Zr/Ti variation. The first evidence is given by the XRD patterns of the samples thermally treated at 900°C. Broadening in the X-ray peaks can be appreciated as the Zr/Ti ratio changes. In Fig. 1, results for y=0.45, 0.53, and 0.60 are shown. The second evidence is obtained by observing the SEM images (Fig. 2), where nice faceted grains are shown. From the microphotographs, it is clear that the largest grain size corresponds to y=0.60, while the lowest size is observed for y=0.45.

Incidentally, the crystallites and the average size are lower than those reported for undoped samples undergoing similar heat treatments [11].

Regarding dielectric features, frequency dependent values of the real and imaginary parts of impedance constitute the total experimental data obtained. Using impedance plots

Table 1 Refinement results for the $Pb_{0.98}Eu_{0.02}(Zr_yTi_{1-y})_{0.995}O_3$ samples.

y	0.45	0.53	0.53	0.60
Space group	P4mm	Cm	R3c	R3c
a (Å)	4.0215(4)	5.7260(2)	5.7473(1)	5.7647(5)
b (Å)		5.7219(1)		
c (Å)	4.1364(5)	4.1154(1)	14.1918(2)	14.221(2)
betha (deg)		90.247(2)		
Weight fraction (%)	100	68(2)	32(1)	100
ρ_{exp}(g/cm^3)	7.63(3)	7.777(7)		7.761(3)
ρ_{exp}/ρ_{th} (%)	95.72	97.85		97.32
Grain size (μm)	1.55	2.57		2.91

Lattice parameters of the R3c phase refer to hexagonal setting.

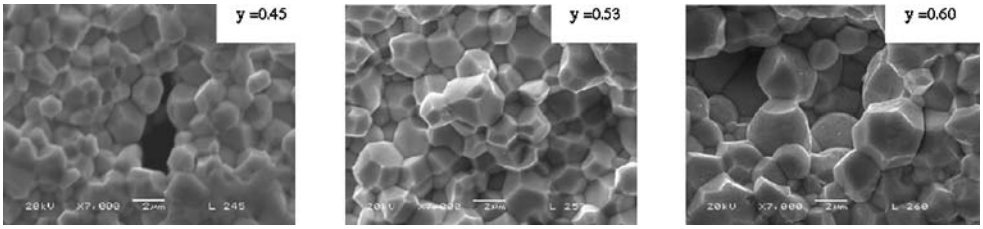

Fig. 2 SEM photographs of $Pb_{0.98}Eu_{0.02}(Zr_yTi_{1-y})_{0.995}O_3$

and modeling via equivalent circuits, may allow determinations of frequency independent parameters related to bulk properties, as has been very often reported [12–14].

However, in our case, at temperatures below 350°C, experimental impedance data were only distributed on the high frequency region. Figure 3 shows impedance curves corresponding to y=0.53, at selected temperatures. Incomplete impedance curves do not allow an appropriate calculation of bulk parameters. Thus, as an alternative procedure, it was decided to use raw data in order to analyze frequency dependent physical features. Figure 4 shows the real part of the dielectric constant $\varepsilon'(\omega)$, plotted as a function of temperature. $\varepsilon'(\omega)$ given by $\varepsilon'(\omega)=gZ''/[\varepsilon_o\omega\{(Z')^2+(Z'')^2\}]$, Z' and Z'' representing the real and imaginary parts of impedance, respectively, g a geometrical factor, ω the angular frequency and $\varepsilon_o=8.854\times10^{-14}$ F/cm. At selected frequencies, curves exhibit a characteristic temperature, indicated by the $\varepsilon'(\omega)$ peak, which corresponds to the expected ferro-paraelectric transition. Peaks are well formed; in all three cases extending in temperature intervals of approximately the same width. The corresponding transition temperatures, T_c, are located at 348, 328 and 307°C, for y=0.45, 0.53 and 0.60, respectively. Evidently, the transition temperature exhibits a Zr/Ti ratio dependence.

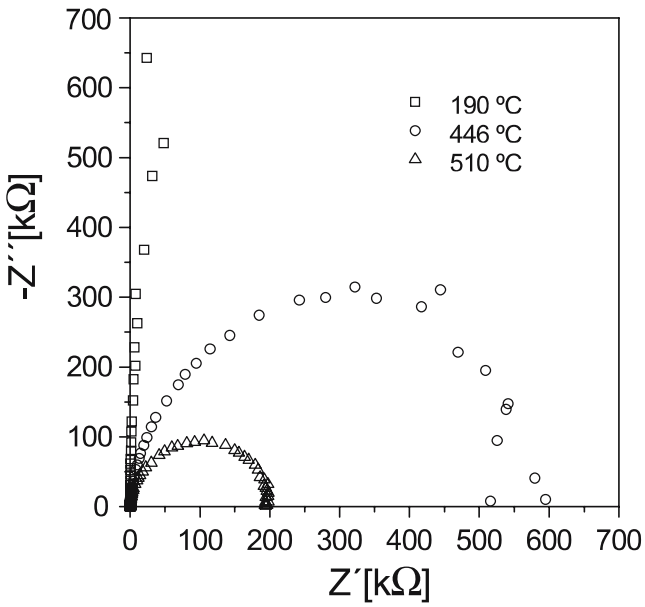

Fig. 3 Impedance curves at selected temperatures, corresponding to y=0.53

Permittivity curves show observable frequency dependence close to T_c. There is a change in the magnitude of $\varepsilon'(\omega)$ for the curves plotted at different frequencies. It is remarkable that, for the sample in which two phases (y=0.53) coexist, the magnitude of $\varepsilon'(\omega)$ is lower than that recorded for the others. On the other hand, given that the $\varepsilon'(\omega)$-peaks for y= 0.45 and y=0.60 appear similar, it is fair to say that the peak dielectric constants of the prepared compounds do not reflect dependence on grain size in this size range. This means that, in those cases where a single phase is present, the dynamic behavior of ferroelectric domains seems to be quite similar, despite the difference in the Zr/Ti ratio values.

Figure 5 shows the temperature and frequency dependence of conductivity, $\sigma'(\omega)$, at selected frequencies. Here, $\sigma'(\omega)$ was obtained by $\sigma'(\omega)=gZ'/[(Z')^2+(Z'')^2]$. In the studied temperature interval, all curves exhibited a significant departure from a straight line. In the low temperature

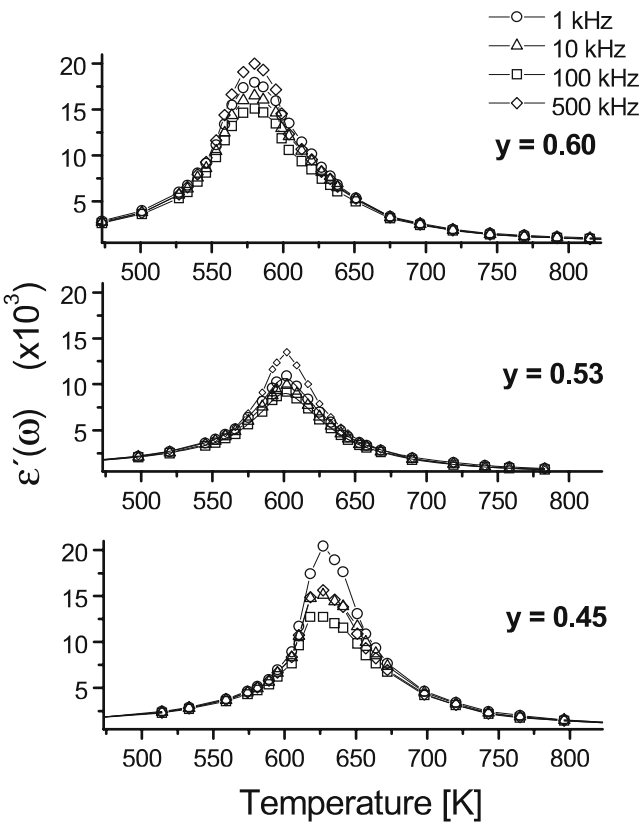

Fig. 4 Real part of the dielectric constant, $\varepsilon'(\omega)$, plotted as a function of temperature

region, and as the temperature rises, an increase in conductivity is observed. However, within a certain temperature interval, $\sigma'(\omega)$ displays a sudden change in inclination, producing a very definite hill. After that, conductivity rises as temperature increases. Evidently, there is a large frequency dependence of $\sigma'(\omega)$, particularly around the observed conductivity hill in Fig. 5. This behavior can be associated with short range processes, properly attributed to the ferroelectric phenomenology. This asseveration is supported by the fact that, in each case, the conductivity hill is formed within the same temperature interval that includes the $\varepsilon'(\omega)$-peak extension (see Fig. 4). Thus, at this stage, the principal source of the registered conductivity must be related to the occurrence of hopping carriers in the physical system. Another observation is that, in the low temperature region, the magnitude of the low frequency conductivity is shorter than that obtained at large frequencies. Naturally, this represents differences reflected in the dynamics of dipolar activity, as a function of frequency. This conductivity is, of course, ac-type. At the very low temperature tail (Fig. 5), the associated activation energy, E_{ac}, was roughly estimated; the results suggesting a gradual decrease in the activation energy values as the frequency goes up.

The maximum value on the conductivity hill is located just at the transition temperatures, and, as mentioned above,

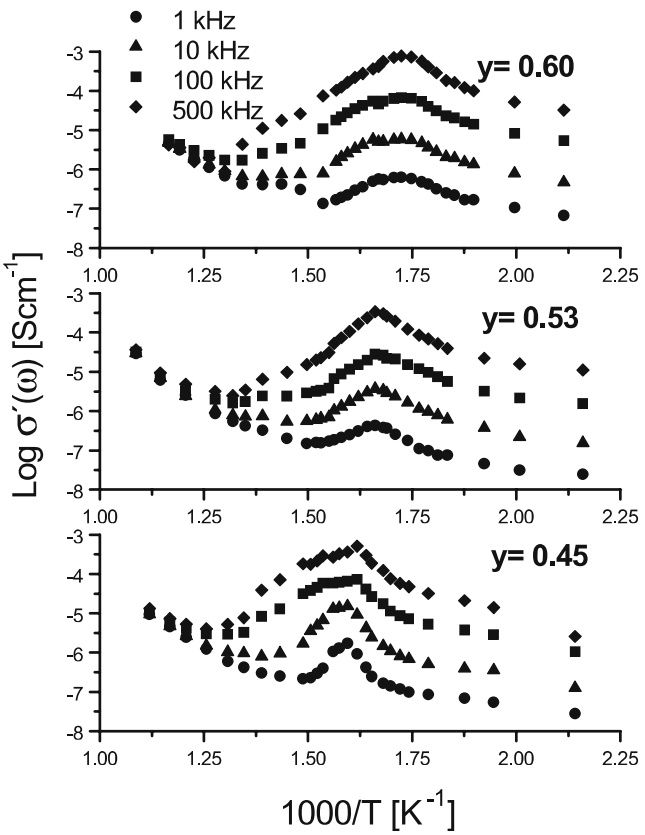

Fig. 5 Temperature and frequency dependence of conductivity, $\sigma'(\omega)$

Table 2 Expressions of σ_{dc}.

$Pb_{0.98}Eu_{0.02}(Zr_yTi_{1-y})_{0.995}O_3$	$\sigma=\sigma_0 e^{-E/kT}$	
y	σ_0 (Scm^{-1})	E (eV)
0.45	160.33	1.28
0.53	7,860.31	1.56
0.60	88.75	1.24

the mechanism of conduction is thought to be associated with the dipolar dynamics. Therefore, due to the crystalline structural change in progress, the decay of conductivity above T_c must be linked to a normal decrease in the dipolar activity. This, in fact, may be reflecting that the probability of the configurational event allowing the formation of an oxygen vacancy nearby a Eu^{3+} ion decreases.

At high temperatures, above the conductivity hill, curves plotted for the different frequencies tend to collapse onto a single curve. Such conductive regimes have been identified [15] with the occurrence of a σ_{dc} component. Conductivity behavior tends to be frequency independent, with the important consequence that, at high temperatures, charge carriers controlling the conductive process must be supplied by a different source than that supplying dipolar activity. It is probable that a long-range process, driven by the temperature field, is responsible for the σ_{dc} component. In the long-range process, it is possible that the promotion of electrons, from the valence band to conductive band, would be involved. The approximate expressions of σ_{dc}, for each composition, are shown in Table 2. These were obtained using data recorded above the conductivity hill. The magnitude of the associated activation energy, E_{dc}, in the high temperature region is larger than the magnitude of the activation energy for the ac process, E_{ac}, in the low temperature region.

The amount of Zr does not show any effect into the conduction behavior. The shape of the curves in Fig. 5 is similar for all the Zr/Ti ratios. However, the Zr quantity does have an effect associated with the phenomenology of the phase transition, as it is shown in Fig. 4.

4 Conclusions

We report a systematic comparative study of the microstructure and dielectric properties, in order to provide a better understanding of phase transition in sol–gel grown doped PZT ceramics. High quality synthesis of $Pb_{0.98}Eu_{0.02}(Zr_yTi_{1-y})_{0.995}O_3$ (y=0.45, 0.53, 0.60) compounds were obtained by a sol–gel route. Products were studied with respect to their crystallographic and dielectric features. In the present work we have reported the effect of adding a fixed amount of Eu^{3+}, for different Zr/Ti concentrations, on the structural and dielectric properties.

X-ray diffraction studies show different crystalline phases corresponding to the perovskite-type structure: tetragonal for y=0.45; monoclinic and rhombohedral for y=0.53; and rhombohedral for y=0.60. From SEM micrographs, a systematic variation in grain size was observed with different Zr/Ti.

In order to investigate the temperature dependence of the dielectric constant, the $\varepsilon'(\omega)$ frequency dependent parameter was used. The shape of $\varepsilon'(\omega)$ vs T curves can be considered typical of a ferro-paraelectric transition. Curves yielded transition temperatures of 348, 328 and 307°C for the worked out compositions y=0.45, 0.53 and 0.6, respectively. At the peak, the magnitude of $\varepsilon'(\omega)$ is similar for the compositions y=0.45 and 0.6, however, the presence of two phases in the compounds for y=0.53 lowers the magnitude of $\varepsilon'(\omega)$. Regarding the temperature dependence of conductivity, which was studied by means of the frequency dependent parameter $\sigma'(\omega)$, it was found that $\sigma'(\omega)$ is strongly influenced by short range processes, particularly at temperatures around and below the transition stage, where it is characterized by a conductivity hill. Therefore, a hopping charge carrier mechanism must be largely responsible for the conductivity at that temperature interval. At the highest measured temperatures, a dc component starts to be defined, by collapsing all frequency dependent conductivities onto a single curve. The associated dc-activation energies are larger than those for the low temperature ac process.

Finally, the amount of Zr does not show any effect into the conduction behavior. The shape of the curves logσ' (ω) as a function of temperature are similar for all the Zr/Ti ratios. However, the Zr quantity does have an effect associated with the phenomenology of the phase transition.

Acknowledgements We wish to acknowledge R. Reyes for his technical assistance. Work supported by DGAPA UNAM IN103603 and, CONACyT-SEP-2004-CO1-47541. We thank the comments of the Referees and their useful observations.

References

1. B. Jaffe, R.S. Roth, S. Marzullo, J. Appl. Phys. **25**, 809 (1954)
2. B. Jaffe, W.R. Cook, H. Jaffe, *Piezoelectric Ceramics*, (Academic, New York, 1971)
3. Y. Xu, *Ferroelectric Materials and Their Applications*, (North Holland, Amsterdam, 1991)
4. J.F. Scott, Ferroelectr. Rev. **1**, 1 (1998)
5. C. Galassi, G. Camporesi, G. Fabbri, A.L. Costa, E. Roncari, J. Eur. Ceram. Soc. **21**, 2011 (2001)
6. Y. Dai, Y. Chen, H. Shen, Z. Zhang, Y. Wang, Ferroelectrics **251**, 77 (2001)
7. G. Yi, Z. Wu, M. Sayer, J. Appl. Phys. **64**, 2717 (1988)
8. S.B. Majumder, B. Roy, R.S. Katiyar, S.B. Krupanidhi, J. Appl. Phys. **90**, 2975 (2001)
9. S.R. Shannigrahi, R.N.P. Choudhary, H.N. Acharya, Mater. Sci. Eng. B **56**, 31 (1999)
10. A. Garg, D.C. Agrawal, Mater. Sci. Eng. B **86**, 134 (2001)
11. W. Cao, C.A. Randall, J. Phys. Chem. Solids **57**, 1499 (1996)
12. J. Ross Mcdonald, *Impedance Spectroscopy: Emphasizing Solid Materials and Systems*, (Wiley, New York, 1987)
13. A.K. Jonscher, *Dielectric Relaxation in Solids* (Chelsea Dielectric, London, 1983)
14. J.T.S. Irvine, D.C. Sinclair, A.R. West, Adv. Mater **2**, 132 (1990)
15. W.K. Lee, B.S. Lim, J.F. Liu, A.S. Nowick, Solid State Ion. **53**–**56**, 831 (1992)